

Robust Optimal Aiming Strategies in Concentrated Solar Tower Power Plants

Sascha Kuhnke^{a,*}, Pascal Richter^b, Fynn Kepp^a, Jeff Cumpston^c, Christina Büsing^a

^a*Lehrstuhl II für Mathematik, RWTH Aachen University, Pontdriesch 10-12, 52062 Aachen, Germany*

^b*Steinbuch Centre for Computing, Karlsruhe Institute of Technology (KIT), Hermann-von-Helmholtz-Platz 1, 76344 Eggenstein-Leopoldshafen, Germany*

^c*Process Systems Engineering, RWTH Aachen University, Forckenbeckstrae 51, 52074 Aachen, Germany*

Abstract

A concentrated solar tower power plant consists of a receiver mounted atop of a central tower and a field of movable mirrors called heliostats. The heliostats concentrate solar radiation onto the receiver where a fluid is heated to produce electricity in a conventional thermodynamic cycle.

Aiming strategies are used to assign each heliostat to an individual aim point on the receiver such that a given flux distribution on the receiver surface is reached. As uncertainties in the tracking of the heliostats exist, aiming strategies are applied that use large safety margins to avoid dangerously high flux concentrations on the receiver. This approach leads to an inefficient use of the power plant and thus economical losses. In this paper, we consider advanced methods to include these uncertainties into the design of efficient aiming strategies. To this end, we present a mixed-integer linear programming (MILP) formulation for the optimization of aiming strategies based on Γ -robustness.

In a case study, we show that the Γ -robust optimization approach yields solutions with strong objective values and thus high economical benefits while maintaining a high degree of safety. Compared to non-robust solutions, the Γ -robust solutions achieve better objective values while guaranteeing the same

*Corresponding author

degree of safety.

Keywords: Solar thermal power, Aiming strategy, Robust optimization, Mixed-integer linear programming, Uncertainty quantification

1. Introduction

The number of solar tower power plants using concentrated solar power (CSP) has increased more than tenfold since 2006 [1]. In CSP plants, large movable mirrors, called heliostats, are used to concentrate rays of sunlight onto a receiver which is mounted on top of a tower. At the receiver, a fluid is heated up. This fluid, typically air, thermal oil or molten salt, transports the heat to a heat exchanger. At the heat exchanger, steam is produced which powers a turbine to generate electricity (see Figure 1).

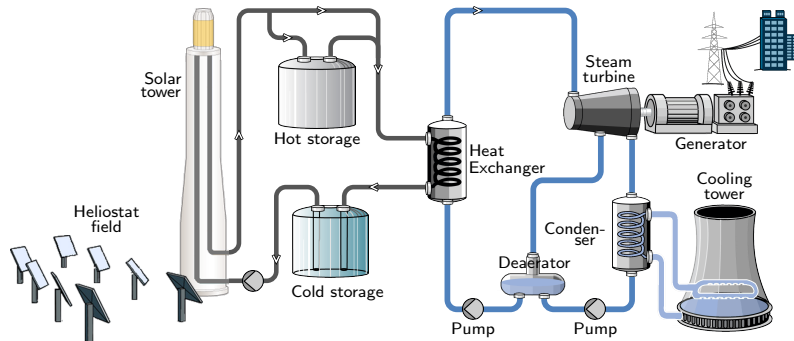


Figure 1: Conceptual drawing of a CSP plant: Large mirrors in the heliostat field concentrate the sun light onto a receiver which is mounted on top of a tower [2].

Concentration ratios of over 2000 suns are possible at the solar receiver. With this high amount of thermal power being intercepted by the receiver, care must be taken that the receiver does not get damaged in the course of operation. A trade-off between maximizing the receiver intercept and minimizing the peak flux on the receiver must be made. In practice, the operator of the power plant pre-computes a desired flux distribution (DFD) across the receiver surface. The task of the aiming strategy is to reach this distribution by directing the

heliostats to aim points on the receiver surface while capturing as much radiation as possible. Here, large safety margins are applied to avoid severe damage of the receiver due to high fluxes caused by tracking errors. A tracking error is an uncertainty that may cause the image of a heliostat at the receiver to be offset
20 from the targeted aim point. Reasons for these offsets are the limited accuracy of the motor in the heliostats and inaccuracies in the whole tracking mechanism. While the safety margins ensure a safe operation, an inefficient use of the entire power plant is accepted.

In this work, we show that a robust aiming strategy which directly considers
25 the uncertainty of the tracking error is able to improve the efficiency while maintaining a high degree of safety. This aiming strategy is found by solving a robust optimization problem formulated as a mixed-integer linear program (MILP).

1.1. State of the art

30 In order to place the current work in context, we present a short description of prior work in which aiming strategies were developed. Previous research on aiming strategies includes the use of specialized heuristics [3, 4, 5, 6, 7], the search for optimized aiming strategies using metaheuristics [8, 9], and the optimization of aiming strategies by solving an MILP formulation [10]. A summary
35 of previous aim point studies is given in Table 1.

Aim point optimization studies go at least as far back as the work included in the DELSOL optics simulation software [3]. There, a set of fixed aiming strategies is proposed in which the aim points of the heliostats are distributed in specific patterns. Six different path dependent heuristics for solving the
40 problem are contained in the DELSOL 2 software release. Here, heuristics for iteratively placing the flux distributions from each heliostat are available for user selection. These include a smart heuristic that fills the receiver surface with the flux profiles until they impinge on the edge of the receiver. The aiming strategies also allow the user to prioritize either the cold end or the hot end of

	Receiver Type	Method	Robustness
[3]	Cylindrical/flat plate	6 heuristics	No
[4]	Flat plate	Operating heuristic	No
[5]	Cylindrical	Heuristic	No
[6]	Cylindrical	6 heuristics	No
[7]	Cylindrical	Heuristic	No
[8]	Flat plate	Ant-colony heuristic	No
[9]	Flat plate	Genetic algorithm	No
[10]	Flat plate	MILP formulation	No
This work	arbitrary	MILP formulation	Yes

Table 1: Summary of previous aim point studies. This work utilizes a robust optimization formulation for the first time in the reviewed literature.

45 the receiver¹.

The complexity of the aim point problem for large heliostat fields is often overcome with the use of simple operating heuristics. For example, García-Martín et al. [4] developed a closed-loop control system using thermo-couples for the circular flat-plate receiver of the PSA CESA-1 plant. The control system balances temperatures by moving heliostats from one aim point of high
50 temperature to one of lower temperature. This is performed iteratively until temperature uniformity is achieved.

A basic heuristic is used for the Gemasolar power plant by Kelly et al. [5] where five possible vertical aim points are allowed and a predefined flux distribution is sought as an objective. This flux distribution is constant in the inner
55 region (about three quarter of the area), and then drops towards the receiver border. The flux distribution in the vertical direction is only considered when choosing aim points for each of the heliostats.

¹Incidentally, this represents an interesting trade-off between high receiver surface temperatures when they are pointed at the hot end, and higher overall thermal losses when they are pointed at the cold end.

In contrast, Astolfi et al. [6] separate the solar field into azimuthal segments
60 and the flux distribution from each segment is optimized. Despite there being
freedom to define the aim point in only the vertical direction, this work accounts
for the influence of the lateral distribution on the ideal vertical aim point distri-
bution in adjacent segments. The best method presented in this paper purports
to reduce peak flux up to 15%. Collado et al. [7] extended this single-parameter
65 aiming approach (the vertical position) to a two-parameter aiming strategy to
flatten the flux profile.

Belhomme et al. [8] propose a solution based on the ant colony optimization
meta-heuristic. This method is able to find solutions in up to 15 minutes.
Different types of receiver constraints such as maximum heat fluxes or maximum
70 heat flux gradients are considered.

The study by Besarati et al. [9] uses a genetic algorithm with the objective
of minimizing the standard deviation of the flux distribution values at each
measurement point on the surface. They considered the PSA CESA-1 heliostat
field, modified by selecting a subset of heliostats such that the peak flux remains
75 within safety limits when all heliostats are pointed at the center of the receiver.

Ashley et al. [10] formulate the aim point optimization as an MILP and
apply this formulation to the PS10 heliostat field. The objective in this case
is to maximize the incident energy on the receiver while reaching a uniform
flux distribution. Optimal flux distributions are found for a range of different
80 operating conditions. The effect of cloud cover is also simulated.

1.2. Our Contribution

In this work, we extend the approach from [10] to first develop a non-robust
MILP formulation for the optimization of aiming strategies. This formulation
additionally allows to approximate a given DFD to further benefit the energy
85 production. Then, we adjust the non-robust formulation to get a robust MILP
formulation for the optimization of aiming strategies based on Γ -robustness [11].
In this robust formulation, uncertainties caused by tracking errors are incorpo-
rated. The design parameter Γ represents the degree of risk aversion against

tracking errors by the operator of the power plant.

90 In a case study applied to the PS10 solar tower power plant, we show that
the resulting robust aiming strategies are superior to the non-robust aiming
strategies. The robust solutions increase both the efficiency and safety of the
plant. Moreover, we conduct a simulation of uncertain tracking errors to show
the practicability of the robust solutions. Our approach is applicable to arbitrary
95 receiver types.

1.3. Outline

First, we describe in Section 2 the underlying problem by defining the opera-
tional variables and design parameters of a solar tower power plant that influence
the optical performance. In Section 3, an MILP formulation for the non-robust
100 optimization of aiming strategies is given. This formulation is extended in Sec-
tion 4 to a Γ -robust MILP formulation which considers uncertainties caused by
tracking errors. In Section 5, we apply the aiming strategies to the solar tower
power plant PS10 in Spain. The solutions of the non-robust and the robust
model are compared and the influence of the robustness parameter Γ on the
105 intercepted solar irradiation is investigated. Finally, we draw in Section 6 a
conclusion regarding the presented aiming strategies and give an outlook with
possibilities to extend this work.

2. Problem Description

This section describes the functionality of a concentrated solar tower power
110 plant along with the optical components which are needed to understand the
purpose and effects of aiming strategies.

2.1. Optical components

A solar tower power plant consists of a *receiver* which is mounted on top of
a tower and a large field of *heliostats*. We denote the set of heliostats by H .
115 The heliostats collect the direct normal irradiation of the *sun* on the Earth's
surface, denoted by I_{DNI} , and reflect it to the receiver. To adapt for the changing

position of the sun, the heliostats are driven by a motor to concentrate the solar irradiation onto the receiver. In our model, the position of the sun is given in terms of the solar zenith and azimuth angle [12]. For the receiver, there exist
 120 three different designs:

- *Flat plate receivers* have a rectangular front shape.
- *Cavity receivers* are curved towards the inside of the tower to minimize heat losses as they are sheltered from wind.
- *External receivers* have a cylindrical shape and are attached at the outside
 125 of the tower.

The receiver consists of a discrete number of panels in a row and the fluid flows along small tubes which are inside these panels. The flow direction is alternating upwards and downwards along the panels. Due to the high power concentration, the material of the receiver has to withstand high temperatures, temperature
 130 gradients in time, and must efficiently transfer the concentrated heat to the flowing medium.

2.2. Aim and Measurement Points at the Receiver

The task of an aiming strategy is to decide for each heliostat at which spot on the receiver surface it should aim. To reduce the difficulty of this task, the aim points on the receiver surface are typically discretized. This means that the heliostats are only allowed to aim at a predefined discrete set of points on the receiver. Here, we use a regular grid as proposed by Ashley et al. [10]. The receiver surface is discretized by the set A containing all possible aim points, i.e.,

$$A = \{a_{i,j} \mid i = 1, \dots, n_a^{\text{horiz}}, j = 1, \dots, n_a^{\text{vert}}\}$$

where n_a^{horiz} and n_a^{vert} are the number of horizontal and vertical aim points. To evaluate an aiming strategy, we measure the heat flux at certain points on the

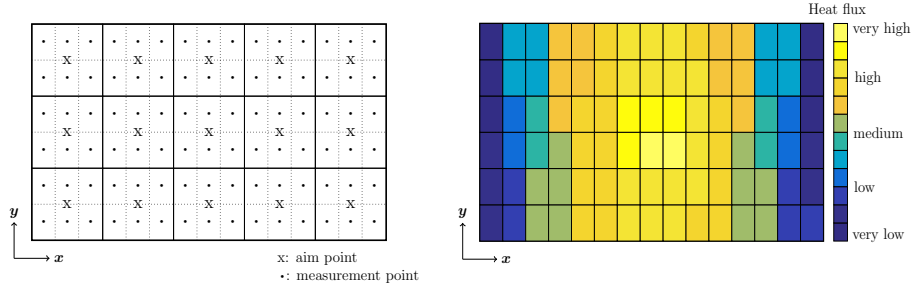


Figure 2: Discretization of aim and measurement points (left) and heat flux distribution on the receiver surface (right).

receiver surface. These measurement points M are arranged in a regular grid similar to the grid of the aim points. It is given by

$$M = \{m_{i,j} \mid i = 1, \dots, n_m^{\text{horiz}}, j = 1, \dots, n_m^{\text{vert}}\}$$

where n_m^{horiz} and n_m^{vert} are the number of horizontal and vertical measurement points. The left hand side of Figure 2 shows a visualization of these discretizations.

135

The set of aim points A is not necessarily the same as the set of measurement points M . In practice, the choice of the number of aim points depends on the relevant flux size of the heliostats. These discretizations can be applied to any receiver shape.

140 *2.3. Desired flux distribution*

Before the optimization of the aiming strategy is conducted, a desired flux distribution (DFD) on the receiver surface is defined which is later used as target of the optimization process. In general, these DFD maps are defined by the operator of the solar tower power plant. They base on CFD simulations conducted by the receiver manufacturer that depend on the receiver material properties and on the possible incident heat flux [13]. The desired flux q_{DFD}^m at the receiver surface is defined point-wise for each measurement point $m \in M$. The right hand side of Figure 2 illustrates a heat flux distribution on the receiver surface which could be used as a DFD map.

145

150 *2.4. Helio­stat flux distribution*

The flux distribution on the receiver surface due to reflection from a particular helio­stat targeting a given aim point can be calculated. Starting in the 1970s, several different methods were developed ranging from straight-forward ray tracing methods to mathematical simulation techniques such as cone op-
155 tics [14], Hermite polynomial expansion or convolution methods [2]. Altogether, there exist several ray-tracing methods which compute the reflected flux distribution of a helio­stat surface onto the receiver surface. The projection on the receiver surface depends on the mirror area, the curvature of the helio­stat, the ray’s angle of incidence with the helio­stat surface (also called cosine efficiency),
160 and on the mirror reflectivity [15].

If helio­stat $h \in H$ aims at aim point $a \in A$, the reflected flux on the receiver surface at measurement point $m \in M$ is given by q_{ha}^m . Since we have a discrete set of aim points, it is possible to pre-compute all possible flux distributions on the receiver for each helio­stat $h \in H$ and each aim point $a \in A$. Hence, we
165 determine one image per helio­stat for every aim point beforehand to save time when performing the optimization. The required memory space for the images depends on the number of helio­stats, the number of aim points and the number of measurement points.

For a certain allocation of helio­stats to aim points, we can now determine
170 the corresponding heat flux distribution on the receiver surface by linearly superposing the reflected fluxes of each helio­stat.

2.5. Allowable Flux Distribution

Due to the nonlinear relationship between radiative thermal losses and heat flux distribution, the relationship between heat flux and receiver surface temper-
175 ature is modelled prior to optimization. When the maximum allowable receiver surface temperature is known, a corresponding maximum allowable flux is calculated and then imposed as linear constraint during the optimization for the best aiming strategy. The maximum heat flux gradient can also be determined

prior to optimization in order to save simulation time. This allows us to formu-
180 late the optimization problem using linear constraints, avoiding the increased
complexity required to solve problems with nonlinear constraints.

The allowable flux distribution (AFD) defines the maximum solar flux allow-
able at any given point on the receiver surface during operation. It is dependent
on the current operating conditions of the receiver. For a receiver that is op-
185 erating in thermal equilibrium, there will be an allowable heat-flux distribution
that corresponds to the differential temperature along the flow direction in the
receiver pipes. The AFD is the maximum solar flux that is allowable under
the given operating conditions such that the temperature of the receiver sur-
face remains within the material limits. Its values are given by q_{AFD}^m for each
190 measurement point $m \in M$.

The AFD is *time dependent*, and a rapidly increasing flux corresponds to a
lower AFD than a slowly increasing flux. This is because the receiver pipe wall
must heat up before the increased flux is conveyed to the fluid in the pipes. Thus,
for a conservative AFD, calculations of the surface temperature resulting from
195 an increase in solar flux shall be performed assuming any extra heat transfer to
the fluid in the receiver be zero.

In the next section, we present a linear formulation of the optimization problem
for finding an optimal aiming strategy based on the here presented model.

3. Non-Robust Aim Point Optimization Model

200 We now present a mixed-integer linear program (MILP) for the optimization
of aiming strategies in solar tower power plants. The purpose is to maximize
the energy production of the whole power plant while preventing damage to
receiver components. In this formulation, we do not consider any uncertainty of
the tracking error. This model is based on the formulation of Ashley et al. [10]
205 with the addition that a given desired flux distribution (DFD) is approximated
to benefit the energy production.

First, we introduce the decision variables used in the optimization formulation. For each heliostat $h \in H$ and aim point $a \in A$, we introduce binary variables x_{ha} which determine if h aims at a . This means x_{ha} is equal to one if h aims at a and zero otherwise.

Now, we consider the constraints of the optimization model. The first set of constraints ensures that each heliostat aims at most at one aim point, i.e.,

$$\sum_{a \in A} x_{ha} \leq 1 \quad \forall h \in H. \quad (1)$$

Here, the left hand side may be zero which represents the situation that a heliostat aims past the receiver in order to avoid damage due to high heat fluxes. The next constraints ensure that the allowable flux distribution (AFD) is satisfied at each measurement point:

$$\sum_{h \in H} \sum_{a \in A} q_{ha}^m x_{ha} \leq q_{\text{AFD}}^m \quad \forall m \in M. \quad (2)$$

In these constraints, the parameters q_{ha}^m are the heat fluxes at measurement point m caused by heliostat h when it aims at aim point a . The parameters q_{AFD}^m are the maximum allowable heat fluxes that must not be exceeded at each m . For the next set of constraints, we consider the desired flux distribution (DFD) which is given by absolute values q_{DFD}^m at each measurement point m . These DFD values depend on the total heat flux currently reaching the receiver. For simplification, we assume that each q_{DFD}^m is equal to a linear expression $q_{\text{DFD}}^m = q_{\text{rel}}^m \cdot \delta$ where $q_{\text{rel}}^m \in [0, 1]$ is a given relative DFD value proportional to q_{DFD}^m and δ is a non-negative continuous variable. The variable δ physically depends on the solar irradiation I_{DNI} and the solar position. Its purpose is to scale the relative values q_{rel}^m . Since the absolute DFD values $q_{\text{rel}}^m \cdot \delta$ can typically not be met exactly, we allow a relative deviation of $\varepsilon > 0$ in both directions from the DFD at each m :

$$(1 - \varepsilon) q_{\text{rel}}^m \delta \leq \sum_{h \in H} \sum_{a \in A} q_{ha}^m x_{ha} \leq (1 + \varepsilon) q_{\text{rel}}^m \delta \quad \forall m \in M. \quad (3)$$

While accepting a relative deviation of ε , these constraints ensure that the resulting heat flux distribution on the receiver surface is close to the DFD.

The objective is to maximize the total heat fluxes at all measurement points $m \in M$ on the receiver caused by the current aiming strategy. Therefore, we optimize the following objective function:

$$\max \sum_{m \in M} \sum_{h \in H} \sum_{a \in A} q_{ha}^m x_{ha}. \quad (4)$$

The MILP presented here for the optimization of aiming strategies has $|H| \cdot |A| + 1$ variables and $|H| + 3|M|$ constraints. However, as the simulation in
 215 Section 5.2 suggests, solutions to this optimization model are very vulnerable against uncertainties caused by tracking errors. Even small deviations of a heliostat from its targeted aim point caused by tracking errors could violate AFD Constraints (2). This poses a high risk of permanent receiver damage. Therefore, we extend this non-robust model by integrating these uncertainties
 220 and computing a robust aiming strategy.

4. Robust Aim Point Optimization Model

Now, we extend the non-robust optimization model to a robust optimization model where we consider uncertainties of tracking errors. A tracking error causes the image of a heliostat at the receiver to be offset from the targeted aim point. These offsets can result in higher heat fluxes than expected which may cause permanent damage to receiver components even though AFD Constraints (2) are satisfied. Therefore, we consider uncertain data and ensure in our model that Constraints (2) are satisfied for all measurement points m with a high probability:

$$\Pr \left(\sum_{h \in H} \sum_{a \in A} q_{ha}^m x_{ha} \leq q_{AFD}^m \right) \geq \eta \quad (5)$$

where q_{ha}^m are now random variables and $\eta \in [0, 1]$ is the degree of certainty that Constraints (2) are actually fulfilled. However, directly solving this stochastic optimization problem is very difficult [16]. Instead, we use a robust optimization
 225 approach to get good feasible solutions for this problem.

Following the approach of Γ -robustness by Bertsimas and Sim [11], we reformulate AFD Constraints (2) by considering default heat fluxes \bar{q}_{ha}^m and their

possible deviations \hat{q}_{ha}^m caused by tracking errors. Since Constraints (2) are upper bounds for the heat fluxes at each measurement point m , it is sufficient to
 230 only consider the worst case deviations towards m and ensure that even in case of such a deviation they remain feasible.

To this end, let \tilde{q}_{ha}^m be the heat flux at m if heliostat h targets aim point a but deviates maximally towards m . Assuming h aims at a , this is the worst case heat flux caused by h at measurement point m . Now, we define \hat{q}_{ha}^m as the worst case deviation from the default heat flux at m , i.e., $\hat{q}_{ha}^m := \tilde{q}_{ha}^m - \bar{q}_{ha}^m$. It follows for each uncertain heat flux q_{ha}^m that it is part of the interval $q_{ha}^m \in [\bar{q}_{ha}^m, \bar{q}_{ha}^m + \hat{q}_{ha}^m]$. However, using a robust approach with worst cases will lead to overconservative solutions since it is highly unlikely that all heliostats assume their worst case deviations at the same time. Therefore, we introduce a parameter $\Gamma \in \{0, 1, \dots, |H|\}$ which represents the maximum number of heliostats that can deviate simultaneously. For each constraint in (2), we want to ensure feasibility if at most Γ heliostats deviate at the same time. In other words, we want to be protected against deviations caused by all possible subsets of heliostats with at most Γ elements. Therefore, we reformulate AFD Constraints (2) as follows:

$$\sum_{h \in H} \sum_{a \in A} \bar{q}_{ha}^m x_{ha} + \text{dev}^m(x) \leq q_{\text{AFD}}^m \quad \forall m \in M \quad (6)$$

where

$$\begin{aligned} \text{dev}^m(x) = \max & \sum_{h \in H} \sum_{a \in A} \hat{q}_{ha}^m x_{ha} \hat{x}_h^m \\ \text{s.t.} & \sum_{h \in H} \hat{x}_h^m \leq \Gamma \\ & \hat{x}_h^m \in \{0, 1\} \quad \forall h \in H. \end{aligned}$$

The value $\text{dev}^m(x)$ is the optimal objective value of another optimization problem. It represents the maximum additional heat flux caused by at most Γ deviations from a given allocation of heliostats to aim points x at a given measurement
 235 point m . However, these reformulated constraints are not linear anymore due to the nested optimization problems.

In the following, we derive a linear reformulation for Constraints (6) following the approach by Bertsimas and Sim [11]. Since the constraint matrix of the inner optimization problem with optimal objective value $\text{dev}^m(x)$ is totally unimodular (consecutive-ones property is satisfied), the corresponding polyhedron is integral. Consequently, relaxing the integrality of the variables \hat{x}_h^m does not change the optimal objective value. This allows us to dualize the inner optimization problem and thus we obtain

$$\begin{aligned} \text{dev}^m(x) &= \min \Gamma z^m + \sum_{h \in H} p_h^m \\ \text{s.t. } z^m + p_h^m &\geq \sum_{a \in A} \hat{q}_{ha}^m x_{ha} && \forall h \in H \\ z^m &\geq 0 \\ p_h^m &\geq 0 && \forall h \in H. \end{aligned}$$

Here, the variables z^m for $m \in M$ and p_h^m for $h \in H$ and $m \in M$ of the dual problem are continuous. As Constraints (6) are upper bounds and we are now minimizing the inner optimization problem, it is equivalent to omit the minimization in the objective. This yields the following linear AFD constraints

$$\sum_{h \in H} \sum_{a \in A} \bar{q}_{ha}^m x_{ha} + \Gamma z^m + \sum_{h \in H} p_h^m \leq q_{\text{AFD}}^m \quad \forall m \in M \quad (7)$$

which eventually replace Constraints (2) in the robust optimization problem. Furthermore, the constraints of the dual optimization problems for each measurement point m are added. Thus, the Γ -robust optimization formulation is

given as follows:

$$\begin{aligned}
& \max \sum_{m \in M} \sum_{h \in H} \sum_{a \in A} \bar{q}_{ha}^m x_{ha} \\
& \text{s.t.} \sum_{a \in A} x_{ha} \leq 1 && \forall h \in H \\
& \sum_{h \in H} \sum_{a \in A} \bar{q}_{ha}^m x_{ha} + \Gamma z^m + \sum_{h \in H} p_h^m \leq q_{\text{AFD}}^m && \forall m \in M \\
& z^m + p_h^m \geq \sum_{a \in A} \hat{q}_{ha}^m x_{ha} && \forall h \in H, m \in M \\
& (1 - \varepsilon) q_{\text{rel}}^m \delta \leq \sum_{h \in H} \sum_{a \in A} \bar{q}_{ha}^m x_{ha} \leq (1 + \varepsilon) q_{\text{rel}}^m \delta && \forall m \in M \\
& x_{ha} \in \{0, 1\} && \forall h \in H, a \in A \\
& \delta \geq 0 \\
& z^m \geq 0 && \forall m \in M \\
& p_h^m \geq 0 && \forall h \in H, m \in M.
\end{aligned}$$

Since the derived AFD Constraints (7) are now linear, the presented Γ -robust formulation is an MILP with $(|H| + 1) |M|$ additional variables and $|H| \cdot |M|$ additional constraints.

240 5. Case Study

In this section, we present a case study which applies the two formulations for the optimization of aiming strategies introduced in Section 3 and 4 to the test field PS10. The results of the non-robust model are compared to the results of the Γ -robust model where different degrees of robustness according to
245 the parameter Γ are considered. Furthermore, a simulation of tracking errors motivates the use of the robust optimization model by showing the vulnerability of solutions of the non-robust model.

First, we state in Section 5.1 the setup of the experiments including the solar tower power plant used in this study, the selected parameters, and specifications
250 about the implementation. In Section 5.2, solutions of the non-robust model are

investigated according to simulated tracking errors. In Section 5.3, we present computational results of the non-robust and robust optimization problem along with detail analysis of the calculated solutions. Finally, a discussion of the results can be found in Section 5.4.

255 *5.1. Setup*

In this case study, we use real data of the PS10 solar tower power plant which is located near Seville, Spain. With a field of 624 heliostats, this plant is being operated commercially from 2007 [17]. Based on the real positions of the heliostats and the receiver [18], we precalculate all expected heat fluxes \bar{q}_{ha}^m and worst case deviations \hat{q}_{ha}^m via ray tracing as described in Section 2.4. We assume that the tracking errors are normally distributed with mean $\mu = 0$ and standard deviation $\sigma = 1$ milliradian (see [19], Section 6.3). For the worst case deviations in the Γ -robust models, we assume a maximum horizontal and vertical tracking error of 1.5 milliradian. In the experiments, we apply a grid of 4 horizontal and 5 vertical aim points along with the same grid of measurement points, i.e., $n_a^{\text{horiz}} = n_m^{\text{horiz}} = 4$ and $n_a^{\text{vert}} = n_m^{\text{vert}} = 5$. We choose a maximum allowable heat flux $q_{\text{AFD}}^m = 200 \text{ kW/m}^2$ at each measurement point m . This value is used because it is exceeded if too many heliostats aim at the same spot on the receiver. Thus, as in larger power plants with more heliostats, a robust approach is necessary to avoid exceeding the AFD. Lastly, we use a maximum deviation $\varepsilon = 10\%$ from a uniform DFD.

For the optimization, we use Java SE Runtime Environment build 1.8.0_191-b12 along with CPLEX 12.8.0.0 [20] with standard options as MILP solver. All numerical results presented here are computed on a Linux machine with an Intel Core i7-3770 CPU with 3.40 GHz clock rate and 32 GB RAM. Calculations are stopped as soon as an optimality gap of 0.5% or the maximum time limit of 7200 seconds is reached. While each non-robust problem terminated within the desired 0.5% gap with a running time of less than 6 seconds, the robust problems terminated after two hours of running time with an average gap of 6.9%. Hence, according to the running time, the non-robust model outperforms

the robust model by magnitudes.

5.2. *The Need of Robustness in the Optimization Model*

First, we evaluate whether a robust approach is necessary to protect the receiver from overheating due to tracking errors. To this end, we test the obtained
285 solutions from the non-robust model introduced in Section 3 against simulated tracking errors.

We denote the non-robust optimization problem introduced in Section 3 by DET. A simple approach to add robustness to this problem is to add buffer values to the AFD Constraints (2). By adding a buffer of $\lambda\%$, $\lambda \in \{0.5, 1, 1.5 \dots, 12\}$,
290 to the right hand sides of these constraints, we obtain a simple robust problem denoted by DET- λ . For each solution of these problems, we perform a simulation by generating 1000 scenarios. Each of these scenarios simulates the deviations caused by tracking errors according to their normal distribution with mean $\mu = 0$ and standard deviation $\sigma = 1$ milliradian. This means that each
295 scenario yields a different actual heat flux distribution on the receiver surface where some of the AFD Constraints (2) could be violated even though they are not violated in the original solution. We say that a scenario is safe if none of the AFD Constraints is violated in its resulting heat flux distribution. For each solution, we denote the number of safe scenarios among the 1000 scenarios by
300 $|S|$. The relative safety of a solution is equal to $|S|/1000$.

The results of the simulation show that the solution to DET has a safety of 0%, i.e., it is violated in all 1000 scenarios and therefore highly unsafe. Adding buffers improves the safety significantly. The solution to DET-5 achieved already a safety of 66%. However, the risk of severely damaging the receiver is still
305 high. The first solution that achieves a safety of 100% is DET-11.5. Here, a high degree of safety for the receiver is guaranteed.

These results show that the solution to DET-11.5 is much more practical than the one to DET since it poses a much lower risk of severely damaging the receiver. However, the objective value of the more robust solution of DET-
310 11.5 is 12% worse than the objective value of DET. Now, the question arises

whether this buffer of 11.5% is suitable. While a high buffer results in poor objective values, a low buffer poses a high risk of severe receiver damage. Furthermore, suitable buffers for each measurement point individually may yield solutions with even better objective values while maintaining a high safety. This is addressed by the more advanced approach of Γ -robust optimization. In Γ -robustness, the degree of robustness is optimized for each measurement point individually as opposed to using the same buffer for all measurement points.

5.3. Performance of Γ -robust Solutions

In this part, we concentrate on the objective values and the safety of the Γ -robust solutions from the model presented in Section 4 in comparison to the non-robust solutions. Besides the non-robust problem DET and the buffer problems DET- λ , we now consider the Γ -robust problems for $\Gamma \in \{0, 1, 2, \dots, 35\}$, denoted by ROB- Γ . For the calculations of the Γ -robust solutions, we first solve ROB-624 by considering it as a non-robust problem with heat fluxes $q_{ha}^m = \bar{q}_{ha}^m + \hat{q}_{ha}^m$ in Constraints (2). Since its solution is also feasible to ROB-35, we use this solution as MILP start. Then, we successively use the solution of ROB- Γ as MILP start for ROB- $(\Gamma - 1)$ until we eventually reach ROB-1.

Figure 3 shows the objective values of the Γ -robust solutions as well as the non-robust and buffer solutions. As expected, the original non-robust problem DET achieves the best objective value. Adding buffers to the non-robust problem yields worse objective values. DET-5 and DET-11.5 already lose about 5% and 12%, respectively, compared to DET. The results of the Γ -robust problems for $\Gamma \in \{0, 1, 2, \dots, 35\}$ show a similar behavior. Increasing Γ and thus a higher robustness yields lower objective values. While ROB-0 is equivalent to DET, the objective value of ROB-1 is already slightly worse. For low Γ values, the loss compared to DET is relatively small. ROB-10 loses only 4% and even ROB-20 results only in an 8% loss. A loss of 12% is reached at $\Gamma = 35$.

In Figure 4, the safety of the Γ -robust solutions in comparison to the non-robust and buffer solutions is depicted. For each solution, we determined its relative safety by simulating 1000 scenarios. As mentioned in Section 5.2, the

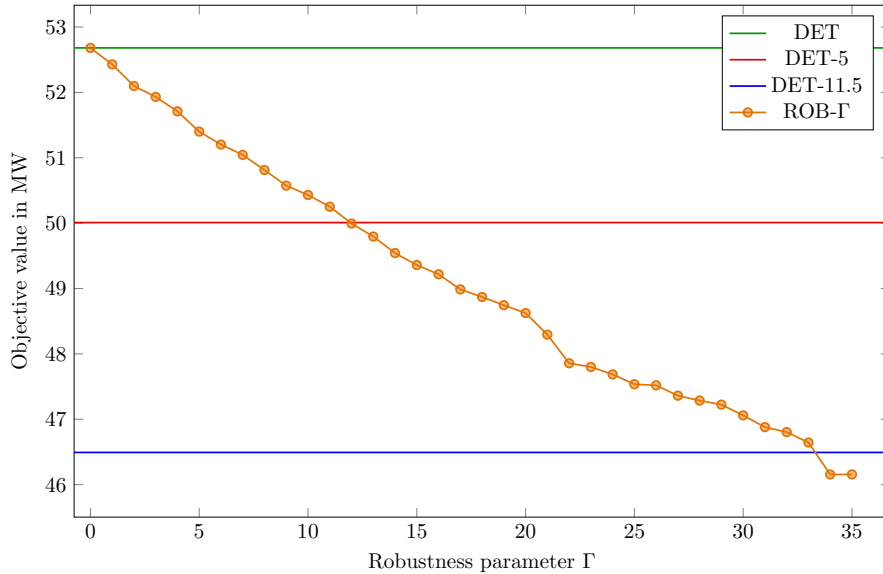


Figure 3: Objective values of non-robust and robust solutions. The objective values decrease as the buffers in the buffer problems and the Γ values in the Γ -robust problems increase.

solution to DET does not provide any safety while the first secure buffer solution is DET-11.5 with a safety of 100%. The Γ -robust solutions show that increasing safety is basically achieved by increasing Γ . While $\Gamma \in \{0, 1, \dots, 4\}$ are violated in all scenarios, ROB-5 is the first solution that has a safe scenario. The safety increases rapidly where ROB-18 already achieves a safety of 96%. A slight safety decrease occurs for ROB-19 and ROB-20 with a safety of 93% each. These decreases are possible because the 1000 randomly generated scenarios are not contained as constraints in the Γ -robust optimization formulation. Subsequently, the safety increases again until the first secure solution with 100% safety is reached at ROB-28.

The objective values and relative safety of the solutions are connected in Figure 5. A Pareto front of these two values is shown for all Γ -robust and buffer solutions. It seems that the buffer solutions are dominating the Γ -robust solutions. Considering the solutions for a safety between 0% and 90%, the buffer solutions have better objective values than the Γ -robust ones while providing a

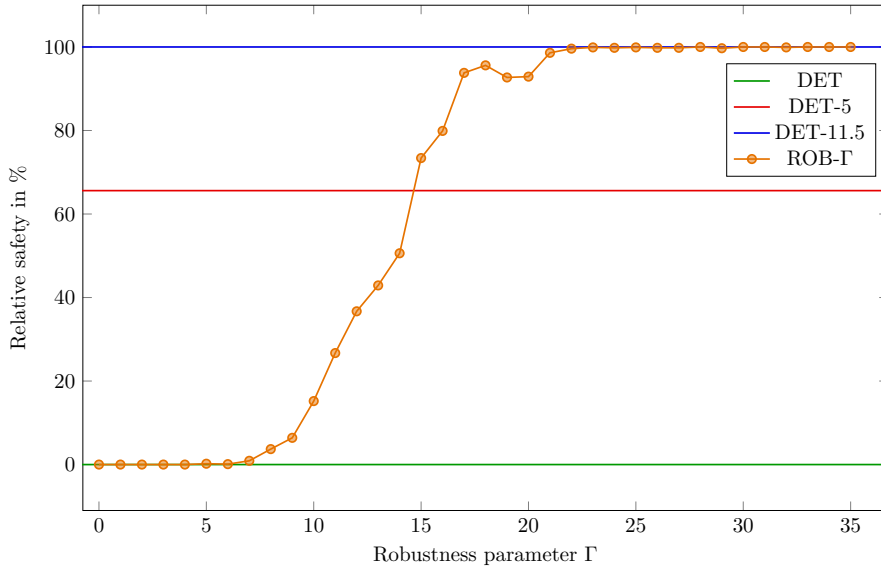


Figure 4: Relative safety in 1000 simulated scenarios. The safety values increase as the buffers in the buffer problems and the Γ values in the Γ -robust problems increase. The first Γ -robust solution with 100 % safety is reached at $\Gamma = 28$.

higher degree of safety. However, these lower safety values are not important in practice because we are only interested in solutions with a very high safety close to 100 %. Therefore, we show in Figure 6 the same Pareto front zoomed to the significant relative safety values. Here, we see that the Γ -robust solutions are very strong when we consider a relative safety close to 100 %. The best objective values along with a safety between 99.5 % and 100 % are all achieved by Γ -robust solutions. They are clearly dominating the buffer solutions where ROB-23 and ROB-28 yield the best objective values for a safety of 99.9 % and 100 %, respectively. For these safety values, this is an improvement in terms of objective value by 2.8 % and 1.7 %, respectively.

Finally, we show the different characteristics of the Γ -robust solutions and the buffer solutions by investigating the slacks of the AFD Constraints (2). Here, the absolute slack S^m at measurement point m is defined as the amount of heat

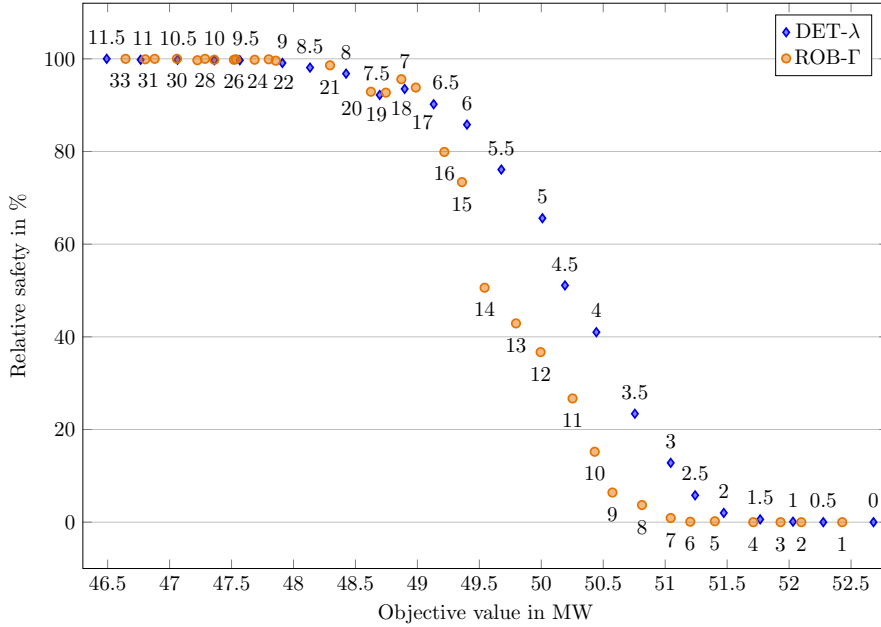


Figure 5: Pareto front of objective values and relative safety. The buffers λ are stated above the buffer solutions DET- λ and the parameters Γ are stated below the Γ -robust solutions ROB- Γ .

flux that we have to add at m to reach the upper bound in Constraint (2), i.e.,

$$S^m = q_{\text{AFD}}^m - \sum_{h \in H} \sum_{a \in A} q_{ha}^m x_{ha} \geq 0.$$

The relative slack s^m at m is given by $s^m = S^m / q_{\text{AFD}}^m$. Figure 7 shows the relative slacks s^m at each m for four selected solutions. The slacks of the solution calculated by DET are shown in Figure 7 (a). All relative slacks of this solution are very small with values of less than 1%. This shows that even small deviations caused by tracking errors could exceed the allowable heat fluxes and cause permanent damage to the receiver. The slacks of DET-11.5, depicted in Figure 7 (b), all lie between 11.5% and 12.8%. It is noticeable that the slacks of DET as well as of DET-11.5 are very homogeneous. On the other hand, the slacks of the Γ -robust solutions show different characteristics. They are not homogeneous anymore. Figure 7 (c) shows the slacks of ROB-23. They lie between 5% and 12.5% while the measurement points with greater slacks are located

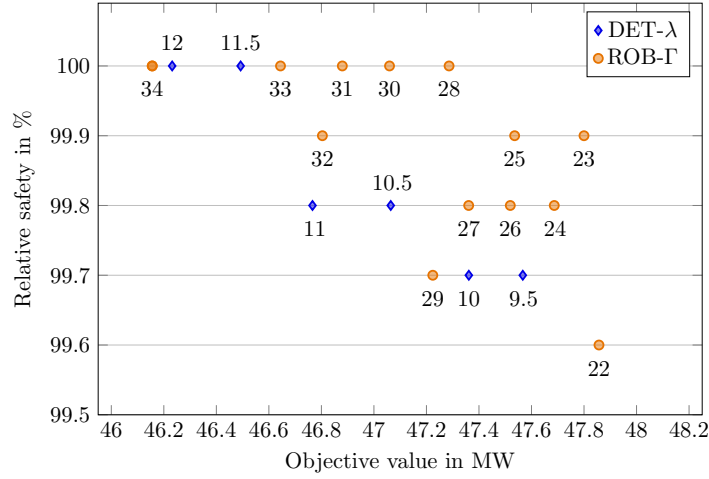


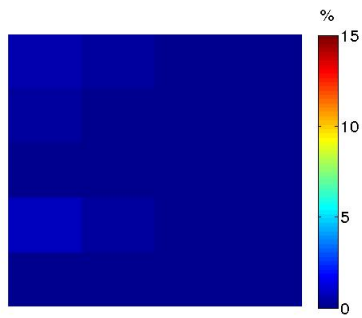
Figure 6: Pareto front zoomed to significant safety values. The buffers λ are stated at the buffer solutions DET- λ and the parameters Γ are stated at the Γ -robust solutions ROB- Γ .

in the center of the receiver and the measurement points with smaller slacks are located at the edge. A similar pattern but with slacks between 5% and 14.5% is given by ROB-28, depicted in Figure 7 (d). This specific distribution of slacks occurs because more heliostats can deviate towards the center than towards the edges which exposes the central points to a higher risk of violation. Consequently, this distribution of slacks allows the Γ -robust solutions to provide more safety while having the same objective values than the buffer solutions.

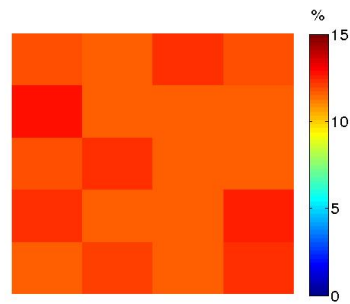
5.4. Discussion of the Results

This computational study shows the benefits of a robust approach for the optimization of aiming strategies in concentrated solar tower power plants. We specify the vulnerability of non-robust solutions as well as the effectiveness of Γ -robust solutions.

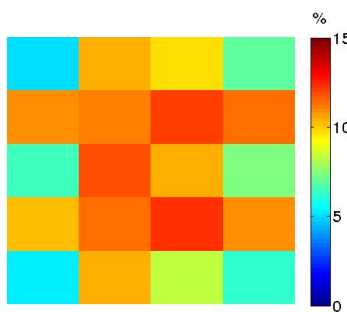
First, we consider a simple robust approach by adding buffer values to the safety constraints. Then, we compare these buffer solutions to the Γ -robust solutions calculated by our Γ -robust optimization model. To evaluate the safety of the solutions, we perform a simulation of the uncertain tracking errors. It turns out that the Γ -robust solutions are superior to the buffer solutions if we



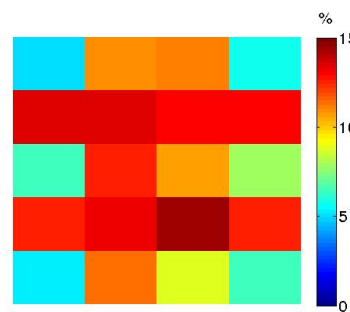
(a) DET



(b) DET-11.5



(c) ROB-23



(d) ROB-28

Figure 7: Relative slacks s^m in AFD Constraints (2). While the slacks in the buffer solutions are very homogeneous, the slacks in the Γ -robust solutions tend to be greater at the central measurement points.

consider the safety values relevant in practice. Finally, we consider the slacks
395 in the Γ -robust solutions which suggest why these solutions are able to provide
more safety than the buffer solutions while having the same objective values.

The Γ -robust approach yields very strong results in terms of objective value
and safety. Additionally, this approach has even more potential because its best
solutions still have an optimality gap of more than 8%. The greatest drawback
400 of the Γ -robust optimization is the running time. Each solution takes a run-
ning time of 7200 seconds compared to 5 seconds of running time of the buffer
solutions. However, with more sophisticated solution approaches, it should be
possible to compute Γ -robust solutions with tighter optimality gaps in signifi-
cantly shorter running time.

405 **6. Conclusion**

This paper presents a robust approach for the optimization of aiming strate-
gies in concentrated solar tower power plants. The goal of this robust approach
is to increase the efficiency and lifespan of such plants. To this end, we first
present an MILP formulation for the optimization of aiming strategies in the
410 non-robust case. Then, we extend this MILP to a Γ -robust optimization formu-
lation which deals with the uncertainty of tracking errors.

We conduct a case study featuring the PS10 solar tower power plant from
Seville, Spain. By performing a simulation of uncertain tracking errors, we
show that a robust approach for the optimization of aiming strategies results in
415 economical benefits. The Γ -robust solutions yield strong objective values while
providing a high degree of safety for the receiver components. Furthermore, we
show that the Γ -robust approach is superior to a simple robust optimization
approach which uses buffers at the safety constraints. Finally, we investigate
the Γ -robust solutions to explain their strength in terms of objective value and
420 safety.

Future research in this area should focus on improving the solutions of the
 Γ -robust optimization model. More sophisticated solution approaches should

be developed to reduce the running times as well as tighten the optimality gaps. Moreover, the Γ -robust approach should be extended to be able to compute
425 robust solutions for large plants with up to 15'000 heliostats surrounding an external cylindrical receiver such as in the Stello solar field Hami in China [21]. Finally, this robust optimization should be incorporated into a dynamic model with regular update steps to be able to cope with dynamic changes like cloud movement.

430 **Acknowledgement**

Funded by the Excellence Initiative of the German federal and state governments.

References

- [1] J. Sawin, et al., Renewable energy policy network for the 21st century
435 renewables 2017 global status report, REN21 Secretariat: Paris, France (2017) 1–302.
- [2] P. Richter, Simulation and optimization of solar thermal power plants, Ph.D. thesis, RWTH Aachen University (2017).
- [3] T. Dellin, M. Fish, C. Yang, User's manual for DELSOL 2: a computer
440 code for calculating the optical performance and optimal system design for solar-thermal central-receiver plants, Tech. rep., Sandia National Labs., Albuquerque, NM (USA); Sandia National Labs., Livermore, CA (USA) (1981).
- [4] F. García-Martín, M. Berenguel, A. Valverde, E. Camacho, Heuristic
445 knowledge-based heliostat field control for the optimization of the temperature distribution in a volumetric receiver, Solar Energy 66 (5) (1999) 355–369.

- [5] B. D. Kelly, Advanced thermal storage for central receivers with supercritical coolants, Tech. rep., Abengoa Solar Inc., lakewood, CO, Report No. DOE/GO18149 (2010).
450
- [6] M. Astolfi, M. Binotti, S. Mazzola, L. Zanellato, G. Manzolini, Heliostat aiming point optimization for external tower receiver, *Solar Energy* 157 (2017) 1114–1129.
- [7] F. J. Collado, J. Guallar, A two-parameter aiming strategy to reduce and flatten the flux map in solar power tower plants, *Solar Energy* 188 (2019) 185–189.
455
- [8] B. Belhomme, R. Pitz-Paal, P. Schwarzbözl, Optimization of heliostat aim point selection for central receiver systems based on the ant colony optimization metaheuristic, *Journal of solar energy engineering* 136 (1) (2014) 011005.
460
- [9] S. M. Besarati, D. Y. Goswami, E. K. Stefanakos, Optimal heliostat aiming strategy for uniform distribution of heat flux on the receiver of a solar power tower plant, *Energy Conversion and Management* 84 (2014) 234–243.
- [10] T. Ashley, E. Carrizosa, E. Fernández-Cara, Optimisation of aiming strategies in solar power tower plants, *Energy* 137 (2017) 285–291.
465
- [11] D. Bertsimas, M. Sim, The price of robustness, *Operations research* 52 (1) (2004) 35–53.
- [12] J. A. Duffie, W. A. Beckman, *Solar engineering of thermal processes*, John Wiley & Sons, 2013.
- [13] A. Sánchez-González, M. R. Rodríguez-Sánchez, D. Santana, Aiming strategy model based on allowable flux densities for molten salt central receivers, *Solar Energy* 157 (2017) 1130–1144.
470
- [14] P. Schwarzbözl, R. Pitz-Paal, M. Schmitz, Visual hffcal - a software tool for layout and optimisation of heliostat fields, in: *SolarPACES Proceedings*, 2009, pp. 1–8.
475

- [15] P. Richter, M. Frank, E. Abraham, Multi-objective optimization of solar tower heliostat fields, in: *Progress in Industrial Mathematics at ECMI 2014*, Springer, 2016, pp. 357–363.
- [16] B. Fortz, M. Labbé, F. Louveaux, M. Poss, Stochastic binary problems with simple penalties for capacity constraints violations, *Mathematical Programming* 138 (1) (2013) 199–221.
- [17] Abengoa Solar Thermal, <http://www.abengoa.com/web/en/negocio/energia/termosolar/> (Accessed 22 August 2019).
- [18] R. Osuna, R. Olavarria, R. Morillo, M. Sánchez, F. Cantero, V. Fernández-Quero, P. Robles, T. López, A. Esteban, F. Céron, et al., PS10, Construction of a 11MW Solar Thermal Tower Plant in Seville, Spain, in: *Solar-PACES Conference*, Seville, Spain, June, 2006, pp. A4–S3, 1–8.
- [19] E. Camacho, M. Soria, F. Rubio, D. Martínez, *Control of Solar Energy Systems*, Advances in Industrial Control, Springer London, 2012.
- [20] IBM, ILOG CPLEX Optimization Studio Release 12.8.0, <https://www.ibm.com/analytics/cplex-optimizer/> (Accessed 22 August 2019).
- [21] T. Keck, M. Balz, V. Göcke, F. von Reeken, F. Gross, W. Landman, J. Collado, J. Salas, J. Gracia, J. Iriondo, et al., Hami—the first stellio solar field, in: *AIP Conference Proceedings*, Vol. 2126, AIP Publishing, 2019, p. 030029.